# Properties of $_{\Lambda}He^4$ *

J. G. Fetkovich,† J. McKenzie,‡ B. R. Riley,§ and I-T. Wang‖
*Carnegie-Mellon University, Pittsburgh, Pennsylvania 15213*

and

M. Derrick, T. Fields, L. G. Hyman, and G. Keyes**
*Argonne National Laboratory, Argonne, Illinois 60439*
(Received 30 June 1972)

In a study of the interactions of stopped negative kaons in a helium bubble chamber, production and decay branching ratios of $_{\Lambda}He^4$ were measured. Relative decay branching ratios agree with earlier results but the production fraction is nearly a factor of two less than the previous measurement. The binding energy of $_{\Lambda}He^4$ was determined from both production and decay reactions. The relationship of the difference between these two binding-energy results to the recent observation of an excited state in $_{\Lambda}He^4$ or $_{\Lambda}H^4$ at 1.09 MeV and the $\bar{K}\Lambda$ parity is discussed.

## I. INTRODUCTION

Studies of the properties of hypernuclei have been of interest primarily because they provide one of the few feasible methods of examining the $\Lambda$-$N$ interaction at low energy. Decay branching ratios, angular distributions, lifetimes, and binding energies are sensitive to the properties of this interaction. Much work has been done on the light hypernuclei (mass numbers 3, 4, and 5) because many of the theoretical problems are more tractable in these cases than for the heavier ones. In addition, hypernuclear reactions have been used in attempts to determine certain basic properties of the elementary particles, such as the $\bar{K}\Lambda$ parity and the nonleptonic decay parameters of the $\Lambda$.

The properties of hypernuclei[1] have been studied using mainly nuclear emulsions and bubble chambers. For light hypernuclei, the helium bubble-chamber technique has an important advantage over the emulsion technique in that only three species can be formed: $_{\Lambda}H^3$, $_{\Lambda}H^4$, and $_{\Lambda}He^4$. There is therefore less difficulty with misidentification, especially since $_{\Lambda}H^3$ and $_{\Lambda}He^4$ events may be identified by production kinematics alone. The complete identification of the production and decay reactions in a bubble chamber allows a determination of production branching ratios which can then be compared to theory, a measurement which is ill-defined in emulsion experiments.

In a helium bubble chamber, there is little problem of mistaking one kind of hypernucleus for another[2]; however, there are backgrounds in some of the topologies studied. These backgrounds are not small in some reactions due to the low production branching fractions for hypernuclei. The high magnetic field used in this experiment was important in the identification and subtraction of these backgrounds, as well as allowing the first determination of hypernuclear binding energy using momentum obtained from curvature.

A unique contribution of this experiment is the first measurement of the $_{\Lambda}He^4$ binding energy at production, as well as at decay. This is of significance with respect to the question whether $_{\Lambda}He^4$ might be produced in an excited state since the ground state is presumably observed in the decay.[3]

The bubble chamber used in this experiment was a cylinder 25 cm in diameter and 36 cm deep with a superconducting magnet which provided a central field of 41 kG. It was exposed to a stopping $K^-$ beam at the Argonne ZGS. The chamber and beam are described in detail in Ref. 4. For this experiment, 118 000 frames were scanned containing 71 400 $K^-$ stops, passing all cuts.

## II. SCANNING AND MEASURING

The production reaction and decay modes studied in this experiment are

$$K^- + He^4 \rightarrow {}_{\Lambda}He^4 + \pi^-, \tag{1}$$

$${}_{\Lambda}He^4 \rightarrow \pi^0 + ppnn \tag{2}$$

$$\rightarrow \pi^- + pppn \tag{3}$$

$$\rightarrow ppnn \tag{4}$$

$$\rightarrow \pi^+ pnnn, \tag{5}$$

where the final-state nucleons in reactions (2)–(5) may emerge bound or unbound. Since only $K^-$ at rest were studied, the production vertex in each event is characterized by a monoenergetic $\pi^-$

TABLE I. Possible decay topologies of $_{\Lambda}He^4$ and their designation in this paper.

| Decay topology | Designation |
|---|---|
| $_{\Lambda}He^4 \rightarrow$ nothing visible | $\pi^0$ |
| $\rightarrow \pi^-$ | $\pi^- 0P$ |
| $\rightarrow \pi^- +1$ prong | $\pi^- 1P$ |
| $\rightarrow \pi^- +2$ prongs | $\pi^- 2P$ |
| $\rightarrow \pi^- +3$ prongs | $\pi^- 3P$ [a] |
| $\rightarrow 1$ prong | $1P$ |
| $\rightarrow 2$ prongs | $2P$ |
| $\rightarrow \pi^+$ | $\pi^+$ |
| $\rightarrow \pi^+ +1$ prong | $\pi^+ 1P$ [a] |

[a] No examples were seen in this experiment.

(~255 MeV/$c$) recoiling collinearly from a $_{\Lambda}He^4$ of range 0.5 mm. The decay topologies observed in this experiment and their designations are listed in Table I. The $\pi^0$ topology is expected to be mainly examples of decay into the final state $\pi^0 He^4$. The $\pi^-$ events are expected to be predominantly decays into the final state $\pi^- p He^3$. The $1P$ and $2P$ decays are collectively called "nonmesonic" since they mainly represent events in which no pion is emitted in the decay.

### A. Carnegie Scanning

Film was scanned according to two distinct sets of rules.[5] The first, called the $A$ scan, was designed to find all $_{\Lambda}He^4$ events regardless of decay topology. The scanners were instructed to follow each beam track until it interacted or left the chamber. Each interaction so found was recorded if it had a $_{\Lambda}He^4$ topology and if it also satisfied the following criteria: The production vertex had to lie within a fiducial area in each view defined to eliminate difficult-to-scan areas and events occurring too near the wall. The sagitta of the beam track had to be within limits appropriate to a stopped $K^-$ track. This requirement helped to eliminate interactions initiated by $\pi^-$ and by in-flight $K^-$. The projected length of the $_{\Lambda}He^4$ track had to be less than 2 mm on the scan table, which was a twice-life-size projection. The $_{\Lambda}He^4$ track and the production $\pi^-$ had to satisfy loose collinearity criteria. It was strongly emphasized that events of marginal acceptability were to be recorded.

It was found that observation of the 0.5-mm $_{\Lambda}He^4$ tracks was especially difficult for those topologies having decay prongs, since the prongs could obscure the short $_{\Lambda}He^4$ track. For this reason, a second set of scan rules was designed to find all $\pi^-$ decay events regardless of the observability of the $_{\Lambda}He^4$ track. In this procedure, called the $2N$ scan, the scanners were instructed to record all events involving two negative tracks (in addition to the beam track) regardless of topology. The procedures were the same as in the $A$ scan, except that no acceptance criteria were applied to the $_{\Lambda}He^4$ track.

Because of the low branching ratio and expected high background rate associated with the nonmesonic decay modes, it was deemed impractical to do an equivalent scan for them.

The sample of film for this analysis was divided into 22 rolls of about 3000 frames each. Each roll was scanned at least once with the $A$ scan and the $2N$ scan. Specifically, five rolls had one $A$ and one $2N$ scan, one had one $A$ and two $2N$ scans, eight had one $2N$ and two $A$ scans, and eight had two $A$ and two $2N$ scans.

### B. Argonne Scanning

Scanning for $_{\Lambda}He^4$ candidates was included in a general scan for $_{\Lambda}He^4$ and $_{\Lambda}H^4$. Each beam track entering the fiducial volume was followed until it interacted or left the chamber. Any interaction producing a negative track which left the fiducial volume was carefully examined as a potential candidate. The event was recorded if in addition it had the following:

1. A collinear stub less than 3 mm in projection (1.5 mm in real space) which (a) did nothing or had a Dalitz pair at decay, or (b) decayed to a negative plus zero to three positive tracks, or (c) decayed to one or two positive tracks and possibly a Dalitz pair.
2. Another negative and zero to three positive tracks at the production vertex.
3. Nothing else at the production vertex.
4. A $\Lambda$ associated with any of the topologies included in 1, 2, and 3.

Sixteen rolls of film were scanned twice using these procedures in which candidates for the decay modes 2 and 3 were not required to have visible hyperfragment track. The Argonne scan thus included both the $A$ and the $2N$ scans done by Carnegie.

### C. Measuring

Acceptable candidates were measured in all three views on manual measuring machines equipped with film-plane digitizers. Measurements of a test reticle yielded an rms error less than 3 $\mu$m on the film. The production vertex was measured for all events. The decay vertex was

measured if the $_{\Lambda}He^4$ track was visible in at least two views.

It was found necessary to limit the measured length of track so that the turning angle of the measured portion was less than about 90°. When this was not done, the geometrical reconstruction program (TVGP) encountered difficulty in fitting a space curve to the measured points. This difficulty is apparently related to the large momentum change along such tracks, as well as to the strong variation of the magnetic field in the chamber (~30% variation within the chamber volume). Even with the turning-angle limitation, the rms deviation on film of the measured points from the projected fitted space curve was often much greater than expected, reaching 10–15 $\mu$m for slow pions.

Possible systematic errors from the magnetic field, fitting programs, or helium density were checked by measuring the $K$ mass from $\tau$ decays, measuring the momenta of $\pi^+$ and $\mu^+$ from $K^+$ decays at rest into $K_{\pi 2}$ and $K_{\mu 2}$ modes, and comparing the momentum of stopped pions as measured from range and from curvature.[6]

## III. PRODUCTION BRANCHING FRACTIONS

### A. Number of $\pi^0$ Events

The principal problems in the determination of the number of $\pi^0$ decay events stem from the fact that the $_{\Lambda}He^4$ track is very short. In order to ensure high detection efficiency for these 0.5-mm stubs, Carnegie scanners were instructed to record an event as $_{\Lambda}He^4$ if there was even a hint of a stub at the production vertex opposite the $\pi^-$. At Argonne, all events with a single $\pi^-$ and no stub were recorded, while events with stubs were subjected to the scanning criteria outlined in Sec. II B. These procedures, of course, increased the number of background events initially included. However, it was expected that the unique momentum of the production $\pi^-$ would serve to determine a clean sample. Other criteria which were used to eliminate background were cuts on the $_{\Lambda}He^4$ length and on the angle between the pion and the $_{\Lambda}He^4$ (expected to be 180°). In order to facilitate an understanding of potential background problems, events were included in the sample even if the production pion momentum was as low as 200 MeV/$c$.

The important cuts applied to each event at the TVGP output level are given in Table II. All events which satisfied these criteria were carefully scrutinized for possible associated $V$'s which were measured and subjected to a three-constraint $\Lambda$ fit using the program SQUAW. Another source of background is caused by $K_{\mu 2}$ and $K_{\pi 2}$ decay events. The background analysis was somewhat different for the Argonne and Carnegie $\pi^0$ samples, so each will be described separately.

TABLE II. Cuts applied to the geometrically reconstructed tracks of the $\pi^0$ events.

| Parameter | Carnegie $\pi^0$ cuts | Carnegie Correction | Argonne $\pi^0$ cuts | Argonne Correction |
|---|---|---|---|---|
| $\lambda_\pi$ = production pion dip | $\lvert\lambda_\pi\rvert \le 60°$ | 1.16 | $\lvert\sin\lambda_\pi\rvert \le 0.8$ | 1.25 |
| $dP_\pi$ = production pion momentum error | $dP_\pi \le 6$ MeV/$c$ | 1.03±0.02 | $dP_\pi \le 6$ MeV/$c$ | 1.23±0.04 |
| $L_K$ = measured kaon length | $L_K \ge 4$ cm | | NA [c] | |
| $L_4$ = measured $_{\Lambda}He^4$ length | $L_4 \le 1$ mm | 1.20±0.04 | $L_4 \le 1.5$ mm | 1.0 |
| $\phi_{K\pi}$ = relative azimuth between $K^-$ and production pion | $70° \le \phi_{K\pi} \le 140°$ | 2.57 | $30° \le \phi_{K\pi} \le 120°$ | 2.0 |
| $K_t$ = kaon $K$ test [a] | $\lvert K_t\rvert \le 2$ | | $\lvert K_t\rvert \le 2$ | |
| $f_K$ = kaon FRMS [b] | $f_K \le 20$ | | NA [c] | |
| $f_\pi$ = pion FRMS [b] | $f_\pi \le 20$ | 1.0 | NA [c] | |
| $\phi_{\pi 4}$ = relative azimuth between pion and $_{\Lambda}He^4$ | $\lvert\phi_{\pi 4} - 180°\rvert/\sigma_\phi \le 2$ | 1.05±0.02 | $\lvert\phi_{\pi 4} - 180°\rvert/\sigma_\phi \le 1.5$ | 1.05±0.09 |
| $\lambda_{\pi 4}$ = relative dip between pion and $_{\Lambda}He^4$ | NA [c] | | $\lvert\lambda_{\pi 4} - 180°\rvert/\sigma_\lambda \le 1.5$ | 1.03±0.09 |
| $dL_4 = L_4$ relative to expected length for $_{\Lambda}He^4$ | NA [c] | | $\lvert L_4 - 0.5$ mm$\rvert/dL_4 \le 2$ | 1.16±0.08 |

[a] This is the TVGP (three-view-geometry program) $K$ test. It is defined so that for stopped tracks it will distribute with a mean of zero and a variance of unity. Tracks interacting in-flight yield $K_t > 0$.

[b] FRMS is the rms deviation of measured track points from the fitted space curve projected onto the film.

[c] NA means this cut was not applied.

### 1. *Carnegie Analysis*

The exclusion of events having $K$-$\pi$ relative azimuth less than 70° (see Table II) was designed to eliminate the $K_{\mu 2}$ background in the region of the ${}_{\Lambda}He^{4}$ peak. With a "$K$ test" $K_t < 2$ corresponding to a beam momentum $\lesssim 125$ MeV/$c$, the maximum possible muon laboratory angle in $K_{\mu 2}$ decay with $P_{\mu} \geq 250$ MeV/$c$ is 69°. That kaon decay events get into the sample is due to delta rays, background bubbles, scanner imagination, and other sources of apparent "${}_{\Lambda}He^{4}$ tracks" at the production vertex.

To search for contamination from kaon decay, all accepted events were fitted to $K_{\mu 2}$ and $K_{\pi 2}$ decay hypotheses. It was found that many did indeed yield $K$-decay fits as did some of the events with fitted $\Lambda$'s. Thus, some of the apparent $K$-decay background is actually due to $\Lambda$ production events in which the $\Lambda$ decayed to $n\pi^0$ and which accidentally fit $K$ decay. We have no evidence that there is any other important background.

The background subtraction is made as follows. Let $N_T$ be the total number of events in the sample, including those fitting $\Lambda$ production and/or $K$ decay. Let $N_K$, $N_\Lambda$, and $N_{K\Lambda}$ be, respectively, the number of (background) events fitting $K$ decay only, $\Lambda$ production only, and $K$ decay and $\Lambda$ production simultaneously. The latter are true $\Lambda$ events which happen to kinematically simulate $K$ decay. Let $n_0$, $n_k$, and $n_\Lambda$ be the true numbers of ${}_{\Lambda}He^{4} - \pi^0$ events, $K$ decays, and $\Lambda$ productions (visible and invisible $\Lambda$'s). Finally, we define the "raw" $\pi^0$ sample, $N_R$, to be the events remaining after the fitted background has been removed. That is,

$$N_R = N_T - (N_K + N_{K\Lambda} + N_\Lambda). \tag{6}$$

Now, we have

$$N_T = n_0 + n_\Lambda + n_k, \tag{7}$$

while

$$n_\Lambda = \tfrac{3}{2}(N_\Lambda + N_{K\Lambda}) \tag{8}$$

and

$$n_k = N_K - \tfrac{1}{2}N_{K\Lambda}. \tag{9}$$

Inserting (8) and (9) into (7) yields

$$n_0 = N_T - \tfrac{3}{2}N_\Lambda - N_{K\Lambda} - N_K,$$

which according to (6) is equivalent to

$$n_0 = N_R - \tfrac{1}{2}N_\Lambda.$$

The production pion momentum distributions for $N_R$, $N_K$, $N_{K\Lambda}$, and $N_\Lambda$ are shown in Fig. 1.

The single-scan efficiency for these events was

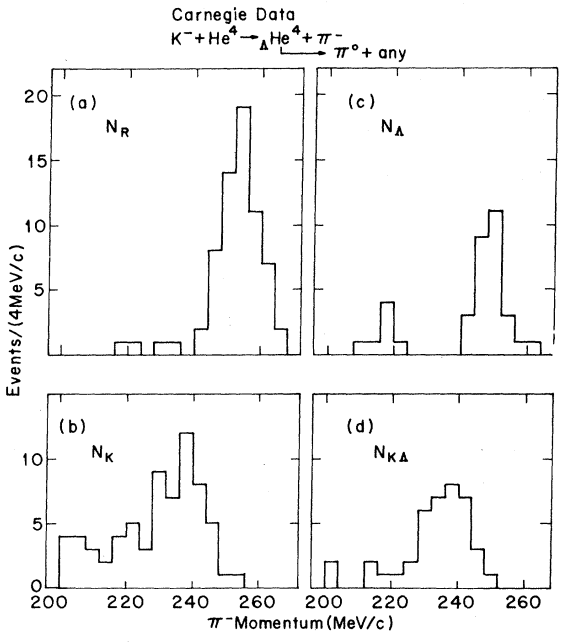


FIG. 1. Distribution in production $\pi^-$ momentum of the Carnegie $\pi^0$-decay candidates. (a) Raw $\pi^0$ sample after the fitted background events were removed. (b) Events fitting $K$ decay only. (c) Events with fitted $\Lambda$. (d) Events with fitted $\Lambda$ also fitting $K$ decay.

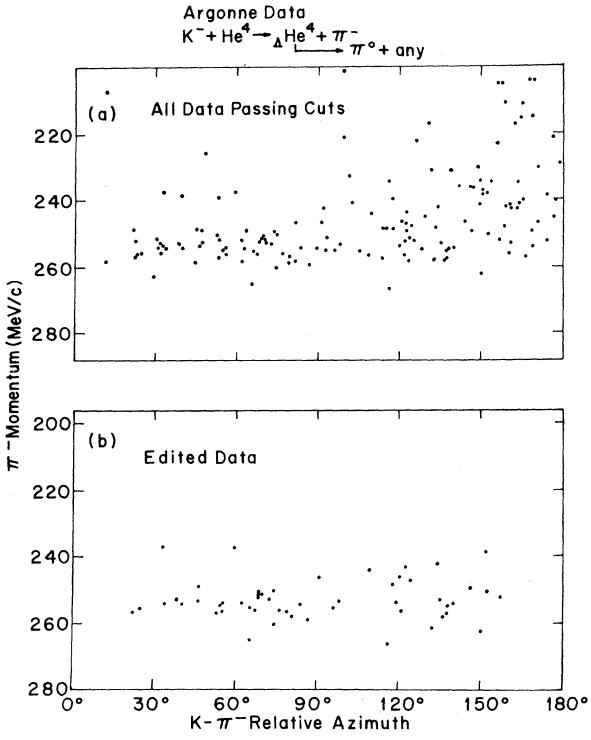


FIG. 2. Scatter plot of production $\pi^-$ momentum versus $K\pi^-$ relative azimuth for Argonne $\pi^0$ decay candidates. (a) All events passing cuts listed in Table II. (b) Events selected from (a) having a clearly visible ${}_{\Lambda}He^{4}$ track.

measured to be $(70\pm7)\%$. Sixteen rolls were scanned twice and six rolls were scanned once to give a total scan efficiency of $(85\pm5)\%$.

The number of stopped $K^-$ in the film was determined by scanning 905 pictures for beam tracks leading to any interaction. These pictures were uniformly distributed throughout the total film scanned in groups of ~75. All events were measured, and the beam track and production vertex were subjected to the same cuts as the $_{\Lambda}He^4$ events.

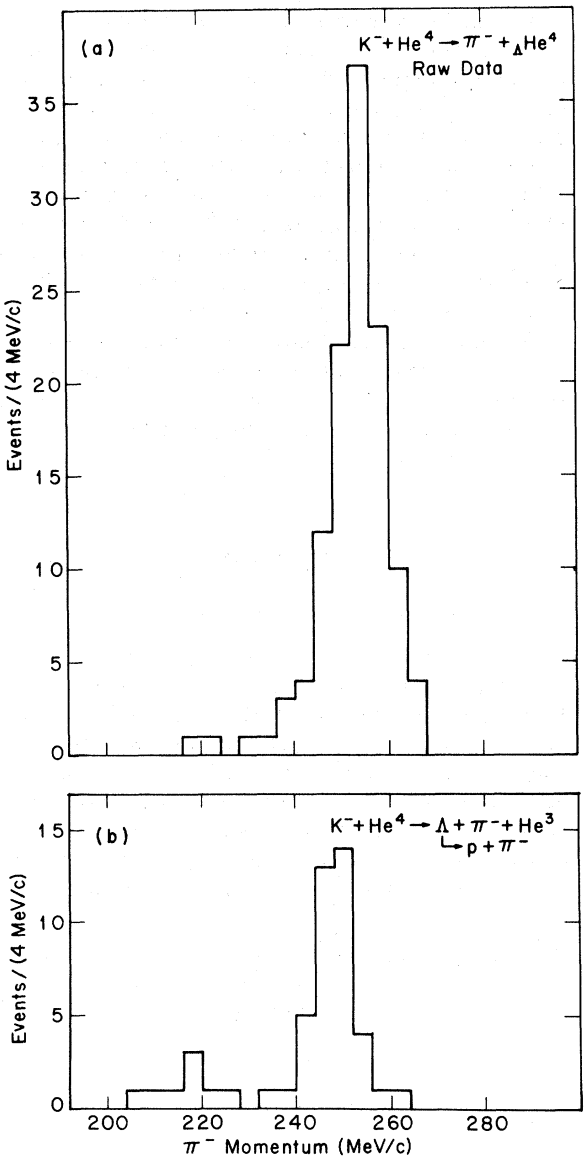


FIG. 3. Distribution in production $\pi^-$ momentum of combined Argonne-Carnegie $\pi^0$-decay candidates. (a) Raw $\pi^0$ sample from Fig. 1(a) and Fig. 2(b). (b) Events with visible fitted $\Lambda$ passing same cuts as those on (a).

When applied to the 22 rolls, the numbers yielded a total of $(40.2\pm1.7)\times10^3$ stopped $K^-$.

### 2. *Argonne Analysis*

The $\pi^0$ data with a visible stub passing the cuts listed in Table II are shown in Fig. 2(a) where the momentum of the production pion is plotted against the relative $K$-$\pi$ azimuth, $\phi_{K\pi}$. There is little evidence in the forward direction for $K_{\mu2}$ decays which would lead to a population of background with $235 \leq P_{\mu} \leq 300$ MeV/$c$. In the backward direction, we see an enhancement caused by the fact that it is easy to imagine a stub when the pion track lies back along the beam track. These events were edited by a physicist and those which contained a definite collinear stub that could be measured on at least two views were retained. The results shown on Fig. 2(b) indicate that information from the 0.5-mm stub is unreliable when it lies within 30° of the beam track in either the forward or backward direction. The number of $\pi^0$ events was estimated from Fig. 2(b) using three different $\phi_{K\pi}$ intervals between 30° and 150°, 120°, 90° and from Fig. 2(a) using $30° \leq \phi_{K\pi} \leq 90°$. All four results were consistent.

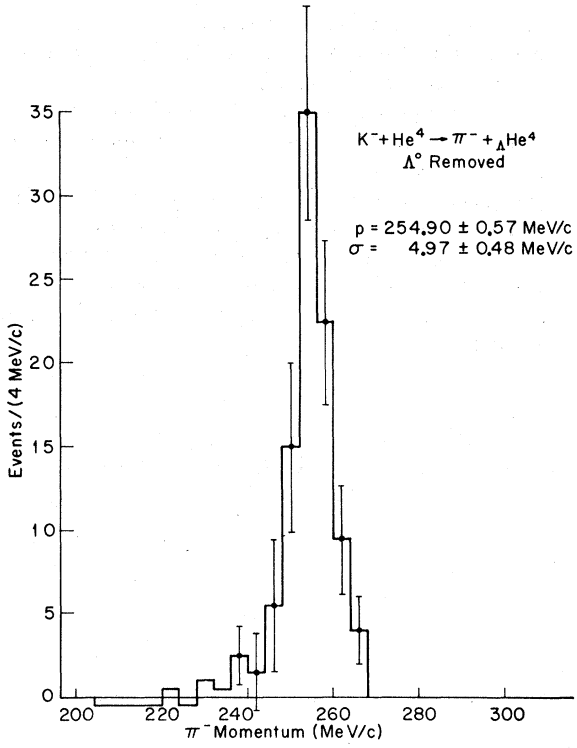


FIG. 4. Distribution in production $\pi^-$ momentum of combined $\pi^0$-decay candidates after all background subtractions. The error bars for those bins in the momentum peak include the effects of background subtractions.

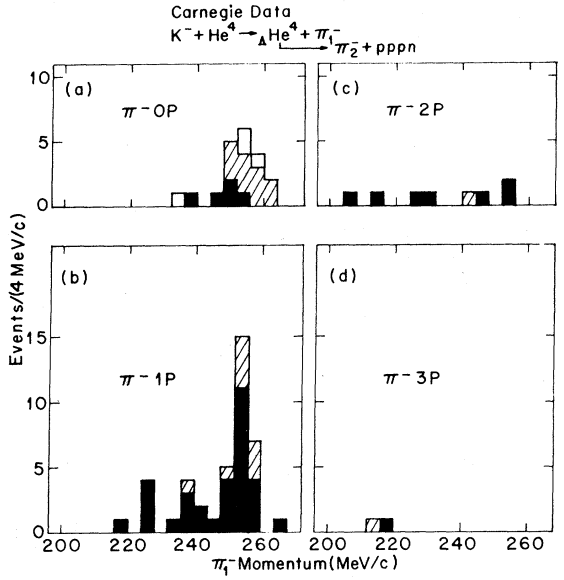


FIG. 5. Distribution in production $\pi^-$ momentum for the Carnegie $\pi^-$-decay candidates. (a), (b), (c), and (d) are respectively the $\pi^-0P$, $\pi^-1P$, $\pi^-2P$, and $\pi^-3P$ topologies. The open areas correspond to events found only in the $A$ scan, the heavily shaded to events found only in the $2N$ scan, and the lightly shaded to events found in both scans.

Events with a visible stub and an associated $\Lambda$ were analyzed in the same way to find the appropriate background subtraction.

The average single-scan efficiency for this topology was $(82 \pm 5)\%$ resulting in a combined efficiency for two scans of $(97 \pm 3)\%$.

Beam tracks were counted every twentieth frame to find the number of stopped $K^-$. One thousand of these events were measured and subjected to the same cuts as the ${}_\Lambda He^4$ events. This procedure yielded $(31.2 \pm 1.0) \times 10^3$ stopped $K^-$ for the 16 rolls scanned.

### 3. Results

The data from Fig. 1(a) and Fig. 2(b) are combined on Fig. 3(a) to give the momentum distribution of the production pion for $\pi^0$ candidates from this experiment. Events with an observed associated $\Lambda$ are shown on Fig. 3(b). After making the subtraction for $\Lambda$'s decaying into the $n\pi^0$ mode, we have the final sample of ${}_\Lambda He^4 \rightarrow \pi^0$ events, with all background removed, on Fig. 4. We find $93 \pm 12$ events in the momentum peak, where the error includes uncertainties due to the background subtractions.

To find the production fraction of ${}_\Lambda He^4$, this number must be corrected for several types of losses. The corrections for effects of cuts are listed in Table II. The dip and azimuth angle distributions were consistent with no losses within the acceptance limits. No correction is required for cuts on the beam tracks since identical cuts were used on the events in the beam count. A 10% correction was made for failures in the reconstruction program. The combined scan efficiency was $(90 \pm 3)\%$.

The product of all the correction factors is $(4.59 \pm 0.33)$ for Carnegie and $(3.96 \pm 0.59)$ for Argonne where the largest portion of the corrections (3.0 and 2.5) are geometric factors from the dip and azimuth cuts on the pion track.

The total number of stopped $K^-$ in the entire experiment is $(71.4 \pm 2.0) \times 10^3$. The branching fraction for the reaction $K^- + He^4 \rightarrow {}_\Lambda He^4 + \pi^-$ with the decay of ${}_\Lambda He^4$ to a $\pi^0$ mode is then $(0.540 \pm 0.071)\%/K^-$ stop.

## B. $\pi^-$ Decays

### 1. Carnegie Analysis

Events undergoing $\pi^-$ decay were originally sought in the $A$ scan described in Sec. II A. These events have one to four tracks emerging from the decay vertex, which is only 0.5 mm from the production vertex. It was expected that events could be systematically missed in the $A$ scan due to obscuring of the ${}_\Lambda He^4$ tracks by one of the decay tracks. As a test, the $2N$ scan was made. Figure 5 shows the production pion momentum spectra

TABLE III. Single-scan efficiencies (in %).

| Decay topology | Carnegie | | Argonne | |
|---|---|---|---|---|
| | $A$ scan | $2N$ scan | Scan 1 | Scan 2 |
| $\pi^-0P$ | $(73 \pm 10)$ | $(76 \pm 10)$ | | |
| $\pi^-1P$ | $(24 \pm 7)$ | $(77 \pm 9)$ | $(84 \pm 8)$ | $(89 \pm 7)$ |
| $\pi^-2P$ | 0 | $(100 \pm 15)$ | | |
| $\pi^-3P$ | | | | |
| $\pi^0$ | $(70 \pm 7)$ | | $(86 \pm 5)$ | $(77 \pm 6)$ |
| $1P$ | $(57 \pm 24)$ | | $(72 \pm 10)$ | $(70 \pm 10)$ |
| $2P$ | $(86 \pm 15)$ | | | |

versus decay topology for the $\pi^-$ events found in the $A$ scan only, the $2N$ scan only, and in both scans. There is evidence that those events having more than one decay track were, in fact, systematically missed in the $A$ scan. This effect is seen more quantitatively in a comparison of the scanning efficiencies of the $A$ scan with those of the $2N$ scan as shown in Table III. Due to this effect, we ignore the $A$ scan for $\pi^-$ events when calculating production fractions.

For the single-scan efficiency, we use the average value over all $\pi^-$ topologies of $(80\pm6)\%$. Nine rolls of this film were scanned twice and 13 rolls were scanned once to give a combined efficiency of $(86\pm4)\%$.

### 2. *Argonne Analysis*

Scanning included all events with two $\pi^-$ and so was not subject to the difficulties of the $A$ scan discussed above. However, there was frequently a discrepancy between the two Argonne scans regarding the specific topology of a given $2\pi^-$ event, e.g., was the $_{\Lambda}He^4$ track visible and were there one, two, or three decay prongs? For this reason, scanning efficiencies were determined for the general $2\pi^-$ class and not for specific decay topologies. The single-scan efficiencies were $(84\pm8)\%$ and $(89\pm7)\%$ giving a combined efficiency of $(98\pm3)\%$ for this mode. The assignment of events to the particular $\pi^-$ decay topologies listed in Table I was made when the events were measured.

### 3. *Results*

The selection criteria applied to these events were in general the same as those applied to the $\pi^0$ events (Table II). Since events were included even if the $_{\Lambda}He^4$ tracks were not visible, there were no cuts on $L_4$ and $\phi_{\pi 4}$. Also, since this topology has no background problem due to $K^-$ decay, the criterion on $\phi_{K\pi}$ was relaxed to $40^\circ \leq \phi_{K\pi} \leq 140^\circ$ and $20^\circ \leq \phi_{K\pi} \leq 160^\circ$ by Carnegie and Argonne, respectively. Dip and azimuth distributions were checked to see that within these limits events were not systematically missed. We also demanded that the energy of the decay pion be consistent with the decay of the $_{\Lambda}He^4$ either at rest or in flight. The over-all correction factor for these cuts is $2.15\pm0.04$ (Carnegie) and $1.76\pm0.06$ (Argonne). The total scanning efficiency was $(91\pm3)\%$.

The combined data for the $\pi^-0P$, $\pi^-2P$, and $\pi^-3P$ decay modes appear on Fig. 6 and the $\pi^-1P$ on Fig. 8. We see in Fig. 6(c) that there are no $\pi^-3P$ decays in our $_{\Lambda}He^4$ sample. Figure 6(b) shows that the number of $\pi^-2P$ events with $P_{\pi_1} > 240$ MeV/$c$ is seven, but two of these have pion momenta $>4\sigma$ away from the expected value 255 MeV/$c$. We thus

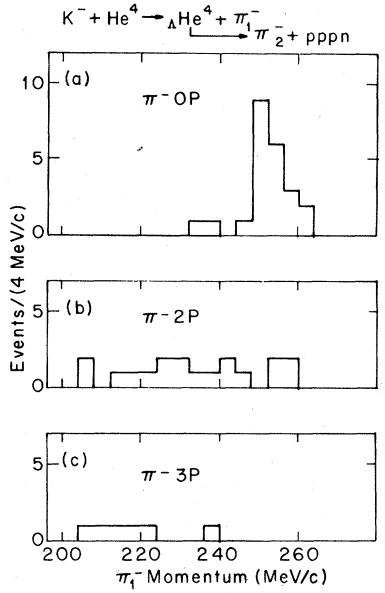


FIG. 6. Distribution in production $\pi^-$ momentum for the combined Argonne-Carnegie $\pi^-$-decay candidates. (a), (b), and (c) are respectively the $\pi^-0P$, $\pi^-2P$, and $\pi^-3P$ topologies.

take $(5\pm2.2)$ as the number of $\pi^-2P$ events and allow for an additional $(1\pm1)$ background events. Using similar arguments, we count from Fig. 6(a) $(21\pm4.6)$ $\pi^-0P$ events in the momentum peak and subtract an estimated background of $(2\pm1)$ events. The number of $\pi^-1P$ events from the momentum projection of Fig. 8 is 72. We remove eight of these which have pion momenta $>4\sigma$ from 255 MeV/$c$; six of these on the low side are $\Lambda$ background while the two on the high side of the peak are consistent with $_{\Lambda}He^4$ production from in-flight $K^-$ with beam momentum ~120 MeV/$c$. We subtract an additional estimated background of $(3\pm2)$ events leaving $(61\pm8)$ $\pi^-1P$ events.

With 71 400 stopped $K^-$ in the film, these numbers yield production branching fractions for $\pi^-0P$, $\pi^-1P$, and $\pi^-2P$ of $(0.059\pm0.016)\%$, $(0.175\pm0.024)\%$ and $(0.012\pm0.008)\%$, respectively. The numbers quoted are percentages of stopped $K^-$ yielding $_{\Lambda}He^4$ decaying into the corresponding topology. These and other branching fractions are summarized in Table IV.

### C. Nonmesonic Decays

The nonmesonic decay modes were selected in $A$-type scans by both Argonne and Carnegie. The Carnegie scanning efficiencies were measured to be $(57\pm24)\%$ and $(86\pm15)\%$ for the one- and two-prong topologies; the Argonne single-scan efficiency for both topologies together was $(71\pm10)\%$. The over-all efficiency for the 38 rolls was thus

TABLE IV. $_{\Lambda}He^4$ production by $K^-$ in liquid helium. The percentages are fractions of stopped $K^-$ leading to $_{\Lambda}He^4$ decaying into the corresponding topologies.

| Decay topology | Production fraction (%) Argonne | Carnegie | Combined |
|---|---|---|---|
| $\pi^0$ | (0.53 ±0.11 ) | (0.55 ±0.10 ) | (0.540±0.071) |
| $\pi^-0P$ | (0.032±0.013) | (0.081±0.024) | (0.059±0.016) |
| $\pi^-1P$ | (0.177±0.032) | (0.173±0.032) | (0.175±0.024) |
| $\pi^-2P$ | (0.011±0.008) | (0.012±0.012) | (0.012±0.008) |
| Total $\pi^-$ | (0.220±0.036) | (0.266±0.041) | (0.246±0.030) |
| Nonmesonic $1P$ | (0.067±0.035) | (0.057±0.030) | (0.061±0.023) |
| Nonmesonic $2P$ | (0.067±0.035) | (0.068±0.027) | (0.068±0.022) – (0.204±0.066) |
| Total nonmesonic | (0.134±0.049) | (0.125±0.040) | (0.129±0.032) – (0.265±0.070) |
| $\pi^+$ | ... | (0.01) | (0.006±0.006) |
| Total all modes | (0.88 ±0.12) | (0.95 ±0.12 ) | (0.92 ±0.08) – (1.06±0.10) |

(88 ± 3)%. The analysis procedures for these events were similar to those for the $\pi^0$ events, and the correction factors to be applied to the raw data are (4.59 ± 0.33) by Carnegie and (4.16 ± 0.25) by Argonne.

Figure 7 shows the production pion spectrum for these topologies. The number of two-prong events with $P_\pi > 240$ MeV/$c$ is 13, but one of these has $P_\pi = 240.8 \pm 3.4$ MeV/$c$ and is thus inconsistent with $_{\Lambda}He^4$ production. We estimate another (1 ± 1) background event leaving (11 ± 3.6) two-prong decays. The one-prong distribution is not as clean as the two-prongs. Of the 15 events with $P_\pi > 240$ MeV/$c$, three have $(P_\pi - 255) > 4\sigma$ and are eliminated as background. We subtract another (2 ± 1) possible background events to give (10 ± 3.7) one-prong decays. These numbers yield branching fractions for one- and two-prong nonmesonic $_{\Lambda}He^4$ decays of (0.061 ± 0.023)% and (0.068 ± 0.017)%, respectively.

Guided by the analysis of the $\pi^-$ decay events, we expect that the $A$-type scan was reasonably effective in finding the one-prong nonmesonic decays, but that the two-prong decays may have been systematically missed due to obscuring of the $_{\Lambda}He^4$ track by one of the secondary prongs. If so, the number of two-prong events should be increased by a factor which can be determined by comparing the $A$ scan and the $2N$ scan results for the $\pi^-0P$ and $\pi^-1P$ events. Figure 5 shows that this factor is ~3, so that the two-prong nonmesonic branching fraction may be as high as (0.20 ± 0.05)%.

### D. $\pi^+$ Decays

One $\pi^+$ decay event satisfying all cuts was found in the Carnegie $A$ scan while no such events survived all the cuts in the Argonne analysis. The one event has a production $\pi^-$ momentum of 254.1 ± 2.6 MeV/$c$ and a decay $\pi^+$ momentum of 90.1 ± 3.4 MeV/$c$. Assuming the correction factor for this topology to be the same as for the others in the $A$ scan, this event corresponds to a branching fraction of (0.006 ± 0.006)%.

## IV. BINDING ENERGY AT DECAY

The decay mode $_{\Lambda}He^4 \rightarrow \pi^- p He^3$ is the dominant $\pi^-$ decay channel. If the proton has sufficient momen-

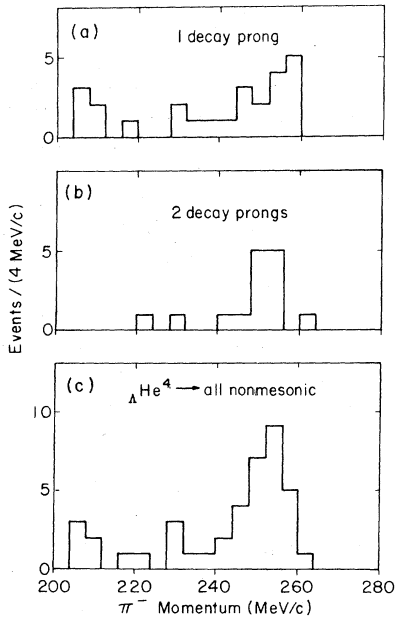


FIG. 7. Distribution in production $\pi^-$ momentum for the nonmesonic-decay candidates. (a) one-prong decays, (b) two-prong decays, and (c) combined one- and two-prong decays.

tum to leave a measurable track, and if the momentum of the $_{\Lambda}He^4$ at decay is known, this reaction may be used to determine the $_{\Lambda}He^4$ mass. The $_{\Lambda}He^4$ momentum cannot be measured with sufficient precision to determine if the hyperfragment decays at rest or in flight. However, the theoretical lifetime of $_{\Lambda}He^4$ implies that ~87% will stop before decay. We have, therefore, calculated the mass for each event assuming the decay occurred at rest. Events which actually decay in flight and pass the cuts yield (Monte Carlo) computed masses averaging ~0.79 MeV high with a spread of ~±1.97 MeV. We expect ~6 events in our sample to be in-flight decays. For this reason, we correct our computed average decay mass downward by $0.11 \pm 0.10$ MeV/$c^2$.

The decays in which the proton track is visible are found in the $\pi^- 1P$ decay topology. A scatter plot of production $\pi^-$ momentum ($P_{\pi 1}$) versus calculated $_{\Lambda}He^4$ mass ($M_4$) for these events is shown in Fig. 8. All the events with $P_{\pi 1} < 244$ MeV/$c$ have momenta $\gtrsim 3\sigma$ from the value expected in $_{\Lambda}He^4$ production and are assumed to be background due to unbound $\Lambda$'s decaying near the production vertex. The seven events satisfying $P_{\pi 1} > 244$ MeV/$c$ and $M_4 > 3927$ MeV/$c^2$ are considered bonafide $_{\Lambda}He^4$ from the $P_{\pi 1}$ values. None of these are examples of $_{\Lambda}He^4 \to \pi^- p He^3$ where the $He^3$ is the visible track and the proton is unseen, since the shortest prong in the group (2 mm) is longer than kinematically allowed for $He^3$. The possibility that they are $\pi^- p He^3$ decays in which the proton has interacted has been considered and rejected on the basis of cross-section estimates. They are evidently $\pi^-$ decays in which the $He^3$ system emerged unbound, and only one proton or deuteron left a visible track.

The 55 events clustered around $P_{\pi 1} = 255$ MeV/$c$ and $M_4 = 3922$ MeV/$c^2$ were used to calculate $M_4$ with the following result:

$$M_4 = 3921.85 \pm 0.22 \text{ MeV}/c^2 .$$

Using $M(He^3) = 2808.34$ MeV/$c^2$ (Ref. 7) and $M(\Lambda) = 1115.59 \pm 0.06$ MeV/$c^2$ (Ref. 6) measured in the same film, we find this corresponds to a $\Lambda$ binding energy,

$$B_{\Lambda}^{d} = 2.08 \pm 0.23 \text{ MeV},$$

where the error includes small contributions from the uncertainties in $M(\Lambda)$ and $M(He^3)$ as well as the statistical error.

We believe this sample to be relatively free of background. However, any background which re-

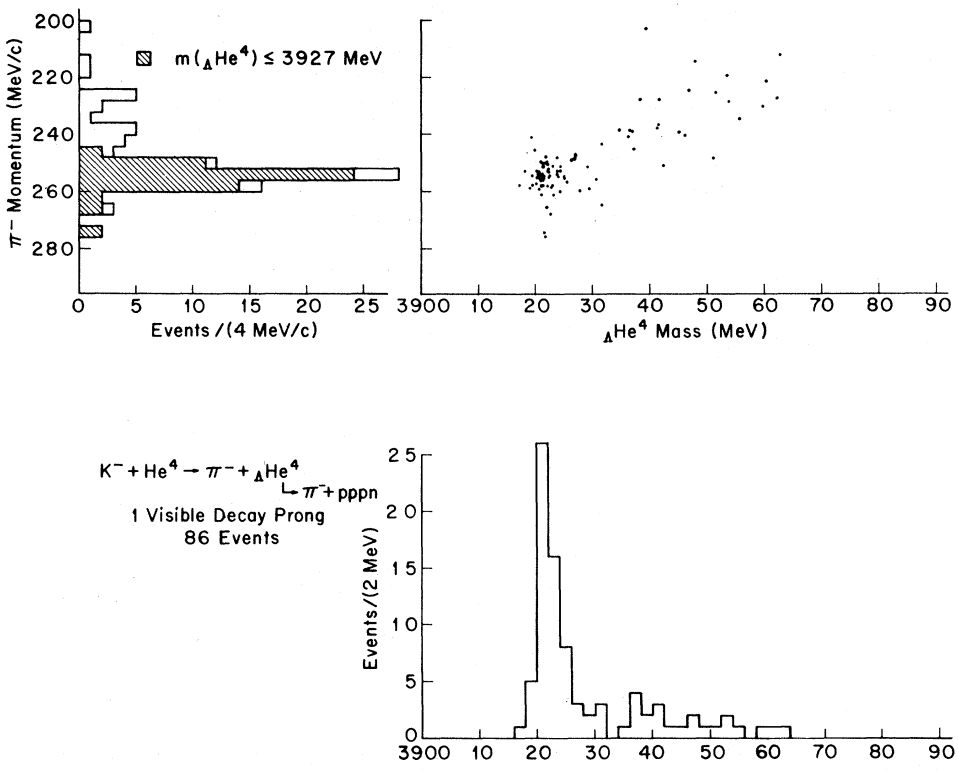


FIG. 8. Scatter plot of production $\pi^-$ momentum versus $M_4$ for the $\pi^- 1P$ topology. $M_4$ is the mass of $_{\Lambda}He^4$ calculated from the decay products assuming the $_{\Lambda}He^4$ decayed at rest and that the final state was $\pi^- p$ $He^3$ with the $He^3$ unseen.

mains may be from the reaction

$$K^- + He^4 \rightarrow \Lambda + \pi^- + He^3$$

near the kinematic limit where the $\Lambda$ and $\pi^-$ recoil from each other and the $He^3$ does not have enough energy to leave a visible track. Furthermore, the most troublesome events are those where the $\Lambda$ opening angle is large, since these can simulate the ${}_\Lambda He^4$ topology even when the $\Lambda$ decay vertex is a few millimeters from the production vertex. To minimize this type of contamination, we remove those events from the sample in which the relative azimuth ($\phi_1$) between the two $\pi^-$ is $<90°$ when the relative azimuth ($\phi_2$) between the decay $\pi^-$ and the decay prong is $>170°$. The result based on 46 events is

$$M_4 = 3921.80 \pm 0.24 \text{ MeV}/c^2$$

which yields

$$B_\Lambda^d = 2.13 \pm 0.24 \text{ MeV}.$$

The correction for decays in flight is $0.11 \pm 0.10$ MeV bringing this to $2.24 \pm 0.27$ MeV.

The sensitivity of $M_4$ to the magnetic field calibration is 0.06 MeV/$c^2$ for 0.1% change in the field. The dependence of $M(\Lambda)$ on the magnetic field was found to be 0.05 MeV/$c^2$ for a 0.1% field change,[6] so these two effects cancel, making $B_\Lambda^d$ independent of the magnetic field. Our final result is thus

$$B_\Lambda^d = 2.24 \pm 0.27 \text{ MeV}.$$

## V. BINDING ENERGY AT PRODUCTION

Since in this experiment we observe ${}_\Lambda He^4$ production by stopped $K^-$, the $\pi^-$ from the production reaction have a unique momentum. A measurement of this momentum provides a determination of the $\Lambda$ binding energy at production. We discuss the event samples used in this determination separately since there are different background problems associated with each decay topology.

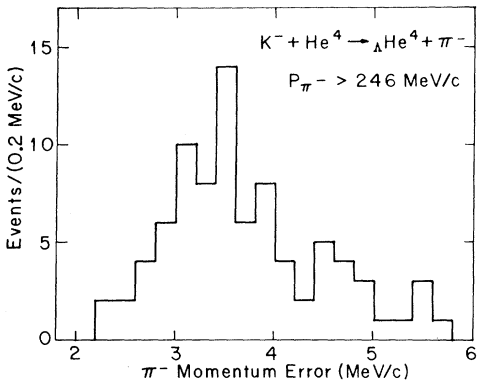


FIG. 9. Distribution of the error in the measured values of $P_{\pi 1}$ for $\pi^0$-decay candidates having $P_{\pi 1} \geq 246$ MeV/$c$.

In dealing with the decay mode $\pi^- 1P$, we use only those events having $P_{\pi 1} > 244$ MeV/$c$ and eliminate those with $\phi_1 < 90°$ when $\phi_2 > 170°$ due to considerations discussed in Sec. IV. These yield a weighted average momentum of $255.53 \pm 0.51$ MeV/$c$.

The sample of $\pi^- 0P$ events seen in Fig. 6(a) includes three events with $P_{\pi 1} < 248$ MeV/$c$ which are $\geq 3\sigma$ below the expected value for ${}_\Lambda He^4$ production and are taken to be background. The remainder are consistent with expectations; however, there might easily be ~2 remaining background events in this sample. To include this possibility, we calculate the average momentum both with and without two background candidates removed. These are chosen to be the two with the lowest $\pi^-$ momenta. The resulting averages are $254.20 \pm 0.78$ MeV/$c$ and $254.45 \pm 0.78$ MeV/$c$. To allow for this uncer-

TABLE V. Production pion momentum and binding energy summary.

| Event type | Argonne | Carnegie | Combined |
|---|---|---|---|
| | Production pion momentum (MeV/$c$) | | |
| $\pi^0$ | $254.80 \pm 0.43$ | $254.86 \pm 0.66$ | $254.86 \pm 0.56$ [a] |
| $\pi^- 0P$ | $252.42 \pm 1.58$ | $254.90 \pm 0.90$ | $254.32 \pm 0.78$ |
| $\pi^- 1P$ | $255.89 \pm 0.72$ | $255.16 \pm 0.73$ | $255.53 \pm 0.51$ |
| $2P$ nonmesonic | $253.72 \pm 1.35$ | $253.69 \pm 1.45$ | $253.71 \pm 0.99$ |
| $1P$ nonmesonic | $255.50 \pm 1.75$ | $254.59 \pm 1.75$ | $255.04 \pm 1.24$ |
| All types combined | $254.89 \pm 0.34$ | $254.85 \pm 0.40$ | $254.91 \pm 0.31$ |
| | | Binding energy (MeV) | |
| $B_\Lambda$ (production) | $1.65 \pm 0.39$ | $1.62 \pm 0.44$ | $1.68 \pm 0.37$ |
| $B_\Lambda$ (decay) | $2.38 \pm 0.34$ | $2.04 \pm 0.38$ | $2.24 \pm 0.27$ |
| Average $B_\Lambda$ | $2.07 \pm 0.26$ | $1.86 \pm 0.29$ | $2.05 \pm 0.22$ |

[a] This value is from a fit to the combined sample of $\pi^0$ decay events and causes the apparent discrepancy between the combined result for all types compared to the mean of the individual Argonne and Carnegie results.

TABLE VI. Relative decay branching ratios for $_{\Lambda}He^{4}$.

| Ratio | Helium bubble-chamber results: This experiment | Helium bubble-chamber results: Ref. 10 | Emulsion results |
|---|---|---|---|
| $\frac{\Gamma(\pi^0+\text{anything})}{\Gamma(\pi^-+\text{anything})}$ | $2.20\pm0.39$ | $2.49\pm0.34$ | |
| $\frac{\Gamma(\pi^- p\,\text{He}^3)}{\Gamma(\pi^-+\text{anything})}$ | $0.87^{+0.06}_{-0.03}$ | | |
| $\frac{\Gamma(\text{nonmesonic})}{\Gamma(\pi^-+\text{anything})}$ | $0.52\pm0.13$ to $1.08\pm0.26$ | $0.52\pm0.10$ | $1.01\pm0.12$ [a]; $\sim1.4$ [b] |
| $\frac{\Gamma(\pi^++\text{anything})}{\Gamma(\pi^-+\text{anything})}$ | 0.03 (one event) | 0.04 (three events) | $0.015\pm0.010$ [c]; $0.054^{+0.015}_{-0.017}$ to $0.069^{+0.018}_{-0.021}$ [d]; $\leq 0.027\pm0.011$ [e]; $0.016\pm0.013$ [f] |
| $\frac{\Gamma(\Lambda p\to np)}{2\Gamma(\Lambda n\to nn)}$ | $1.7\pm0.9$ | $1.1\pm0.4$ | |

[a] K. N. Chaudhari, S. N. Ganguli, N. K. Rao, M. S. Swami, A. Gurtu, J. M. Kohli, and M. B. Singh, Proc. Ind. Acad. Sci. 69A, 78 (1969).

[b] J. Sacton, in *Proceedings of the International Conference on Hyperfragments, St. Cergue, 1963* (CERN, Geneva, 1964), p. 53.

[c] K. N. Chaudhari, S. H. Ganguli, N. K. Rao, M. S. Swami, A. Gurtu, J. M. Kohli, and M. B. Singh, Proc. Ind. Acad. Sci. 68A, 228 (1968).

[d] G. Bohm, J. Klabuhn, U. Krecker, F. Wysotzki, G. Coremans, C. Mayeur, J. Sacton, P. Vilain, G. Wilquet, D. O'Sullivan, D. Stanley, D. H. Davis, E. R. Fletcher, S. P. Lovell, N. C. Roy, J. H. Wickens, A. Filipkowski, K. Garbowska-Pniewska, T. Pniewski, E. Skrzypczak, T. Sobczak, J. E. Allen, V. A. Bull, A. P. Conway, A. Fishwick, and P. V. March, Nucl. Phys. B9, 1 (1969).

[e] M. J. Beniston, R. Levi-Setti, W. Puschel, and M. Raymund, Phys. Rev. 134, B641 (1964).

[f] R. E. Phillips and J. Schneps, Phys. Rev. 179, 1292 (1969).

tainty in background subtraction, we use a value $254.32\pm0.78$ MeV/$c$ when calculating an average binding energy at production.

The $\pi^-2P$ decay events on Fig. 6(b) seem to be too contaminated to be useful for measuring the production binding energy.

The one-prong and two-prong nonmesonic events are treated similarly to the $\pi^-0P$, allowing for 2 and 1 additional background with production pion momenta less than three errors from the expected value for $_{\Lambda}He^{4}$ production. These two modes give weighted averages of $255.04\pm1.24$ MeV/$c$ and $253.71\pm0.99$ MeV/$c$, respectively.

The $\pi^0$ decay events may also be used to determine the binding energy at production; however, one cannot just compute a weighted average of individual events because the subtraction of unseen $\Lambda$ events is done statistically. To determine the central momentum, a Gaussian curve was fitted to the part of the distribution in Fig. 4 between 236 and 268 MeV/$c$. In making the fit, the error assigned to the number of events in each bin included the effect of the uncertainty in the background subtraction.

The fit was done in two ways. First, the standard deviation of the Gaussian, $\sigma$, was fixed at 3.6 MeV/$c$ on the basis of the distribution of production pion momentum errors shown in Fig. 9. In the second fit, $\sigma$ was left as a free parameter. The normalization and central value of the Gaussian were parameters in both fits. The fits yielded central values differing by $0.19\pm0.83$ MeV/$c$. The normalizations were $(86\pm11)\%$ and $(95\pm13)\%$ with $\chi^2$ of 8.6 and 4.3 for 6 and 5 degrees of freedom, respectively. The second fit yielded $\sigma=4.81\pm0.56$ MeV/$c$. We use the mean pion momentum determined from the three-parameter fit for the $\pi^0$ decay events, which is $254.86\pm0.56$ MeV/$c$.

A summary of results of the average production pion momenta for the various topologies is given in Table V. These yield a mean binding energy at production, $B_{\Lambda}^{p}$, of $1.68\pm0.32$ MeV.

We add to this error an amount due to the uncertainty in the magnetic field calibration. We have checked the magnetic field in several ways described in Ref. 6 and find an uncertainty of $\pm0.1\%$. We may also use the world average[8] for $M(\Lambda)$, excluding our value in Ref. 6, along with our measured derivative $\delta M(\Lambda)/\delta H$, to provide an independent calibration of the field. This yields an uncertainty of $\pm0.13\%$ which can be combined with our result to give an over-all magnetic field uncertain-

ty of ±0.08%. This produces a contribution of 0.19 MeV to the binding-energy uncertainty, giving finally

$$B_\Lambda^p = 1.68 \pm 0.37 \text{ MeV}.$$

## VI. DISCUSSION OF RESULTS

### A. Production and Decay Branching Ratios

The frequencies for stopped $K^-$ producing ${}_\Lambda He^4$ decaying into the various possible decay modes are given in Table IV. In an earlier helium bubble-chamber experiment,[9] the production branching ratio for ${}_\Lambda He^4$ was measured to be $(1.8 \pm 0.5)\%$ based on an analysis of 1141 stopped $K^-$. The result from this experiment using 71 400 stopped $K^-$ is $(0.99 \pm 0.09)\%$ per $K^-$ stop.

We find generally good agreement when we compare the relative decay branching ratios with those of the previous experiment.[10] One discrepancy occurs in the $\pi^- 0P$ mode which we measure to have a decay branching fraction of $(6 \pm 2)\%$ compared to $(2 \pm 1)\%$ measured in Ref. 10. This is most likely due to an arbitrariness in the definition of a prong. In this experiment, decay tracks shorter than 0.5 mm are likely not to be counted as prongs, which leads to some reshuffling of events among topologies. The ratios for $\Gamma({}_\Lambda He^4 \to \text{all } \pi^-)/\Gamma_{\text{tot}}$, on the other hand, agree well: $(25 \pm 3)\%$ from this experiment versus $(25 \pm 3)\%$ from Ref. 10.

Various decay branching ratios derived from Table IV are compared with results from other experiments in Table VI.

The value of $\Gamma(\pi^- p He^3)/\Gamma(\pi^- + \text{anything})$ has been measured for the first time in this experiment.

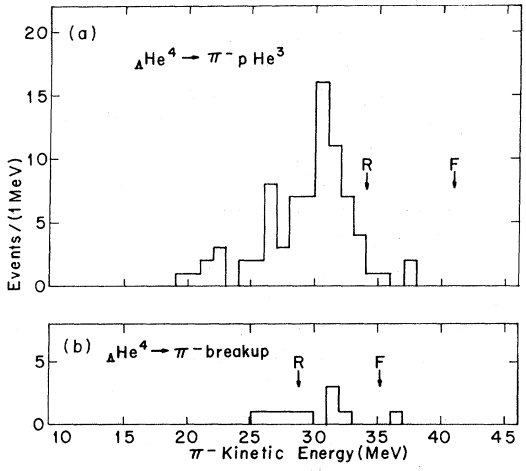


FIG. 10. Distribution in kinetic energy of the decay $\pi^-$ for (a) ${}_\Lambda He^4 \to \pi^- p He^3$ events and (b) ${}_\Lambda He^4 \to \pi^-$ breakup events. The arrows indicate the maximum allowed energies for the decay $\pi^-$ when the ${}_\Lambda He^4$ decays at rest ($R$) and in flight ($F$).

All $\pi^- 0P$ events were classified as $\pi^- p He^3$ decays, while all $\pi^- 2P$ were classified as breakup events, since they were found not to fit the $\pi^- p He^3$ decay hypothesis even allowing decay in flight. Those $\pi^- 1P$ events in the mass peak of Fig. 8 were called $\pi^- p He^3$ decays, and those outside the mass peak, but in the momentum peak, were called breakup events (see Sec. IV).

The energy distribution of the decay $\pi^-$ for $\pi^- p He^3$ events is shown on Fig. 10(a). The shape of the spectrum agrees with results from nuclear emulsion.[11] Figure 10(b) displays the $\pi^-$ energy distribution for the breakup events. We see from the latter figure that ~5 of the breakup events are apparently from ${}_\Lambda He^4$ decays in flight, whereas we expect only ~1 in this sample. When calculating the fraction of $\pi^- p He^3$ events among all $\pi^-$ decays, we have, therefore, enlarged the upper error to allow for an additional four background events.

The nonmesonic decay events are presumed to be examples of the induced $\Lambda$ decay reactions:

$$\Lambda + n + (pp) \to n + n + (pp)$$

and

$$\Lambda + p + (pn) \to n + p + (pn),$$

where the particles in parentheses act as spectators.

We may attempt to distinguish between these two reactions by noting that proton-induced decays will tend to have fast protons emerging (~400 MeV/$c$). The momentum distribution obtained from the nonmesonic events when the longer prong is interpreted as a proton is shown in Fig. 11. The clustering at 400 MeV/$c$ is evident. Spectator nucleons are expected to be distributed roughly according to the indicated Fermi distribution. To allow a comparison to existing data,[10,12] we count the five lowest-momentum events as neutron induced, leaving

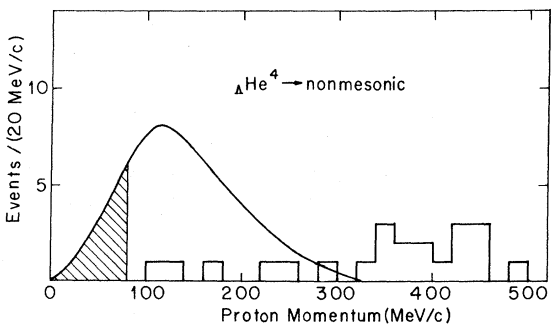


FIG. 11. Distribution in momentum of the longer prong interpreted as a proton from the nonmesonic-decay events. The Fermi distribution for $He^4$ is shown for comparison. Protons in the shaded region would leave tracks too short to be detected.

TABLE VII. Summary of $\bar{K}\Lambda$ parity, hypernuclear state, and capture wave of kaon.

| $\bar{K}\Lambda$ parity | | Even | | Odd | |
|---|---|---|---|---|---|
| Capture wave | Hypernucleus $J^P$ at production | $0^+$ | $1^+$ | $0^+$ | $1^+$ |
| $s$ | | Forbidden | Allowed | Allowed | Forbidden |
| $p$ | | Forbidden | Allowed | Allowed | Allowed |

17 proton-induced decays. Given the two-to-one ratio of protons to neutrons in $_{\Lambda}He^4$, this arbitrary separation is equivalent to an induced decay ratio per nucleon of

$$\frac{\Gamma(\Lambda p \to np)}{2\Gamma(\Lambda n \to nn)} = 1.7 \pm 0.9 .$$

The error is statistical only and does not include any systematic allowance for the crudeness of the model.

The large momentum transfer in the nonmesonic decays makes it unlikely that two-body decays will occur. One model[13] predicts the fraction of all nonmesonic decays into the two-body modes $He^3n$ and $H^3p$ to be 1.5% each. Two emulsion experiments observe no examples of $_{\Lambda}He^4 \to H^3p$ but do find $_{\Lambda}He^4 \to He^3n$ in the ratios $(0.08 \pm 0.04)$ (Ref. 14) and $(0.14 \pm 0.05)$ (Ref. 15) compared to all uniquely identified nonmesonic decays of $_{\Lambda}He^4$. We have found no examples of these modes or $_{\Lambda}He^4 \to dd$ in our sample.

### B. $\bar{K}\Lambda$ Parity

The relative $\bar{K}\Lambda$ parity may be measured by observation of the reactions[16]

$$K^- + He^4 \to {}_{\Lambda}He^4 + \pi^-$$
$$\to {}_{\Lambda}H^4 + \pi^0 .$$

Since the spin and parity of the $K$ and $\pi$ are $0^-$ and $He^4$ is $0^+$, the $\bar{K}\Lambda$ parity is odd if the spin of the hypernucleus is $0^+$. This is true even though the $K^-$ meson may be captured from $s$ or $p$ atomic states. If, however, the hypernucleus is produced in an excited $1^+$ state, then no conclusion can be drawn about the parity unless one can prove that the initial capture proceeds from an atomic $s$ state. These statements are summarized in Table VII.

The only evidence on the spin of the hypernucleus at production is the measurement of the production ratio of $K^-$ in helium,

$$R = \frac{\Gamma(_{\Lambda}He^4 + \pi^-)}{\Gamma(_{\Lambda}He^4 + \pi^-) + \Gamma(\Lambda + He^3 + \pi^-)} .$$

This ratio was calculated by Dalitz and Downs[17] to be 15% for production of the ground state and 2% for the excited state assuming atomic $s$-state capture of the $K^-$ and an $s$-wave $\bar{K}N$ interaction. Using a different model, Block[18] calculated 14% and 15% for ground-state production of $_{\Lambda}He^4$ from $s$- and $p$-state atomic orbits and $\lesssim 5\%$ for the excited state. All of these calculations for the production of the excited state were done on the assumption that the excited-state binding energy was $B_{\Lambda}^* \cong 0.1$ MeV, and the ratio is expected to vary as $(B_{\Lambda}^*)^{1/2}$. Recent analyses of the $\Lambda N$ interaction[19] indicate the excited state is probably bound by more than 1 MeV. This is corroborated by a recent experiment[20] which reported the observation of a 1.09-MeV x ray from the deexcitation of $_{\Lambda}He^4$ or $_{\Lambda}H^4$ and a possible additional line at 1.42 MeV. Taking $B_{\Lambda}^* = B_{\Lambda}^d - E_{\gamma} = 1.22$ MeV, the values of $R$ expected for the excited-state production are ~7% and ~17% in the two models.

This ratio has been measured by Block *et al.*[10] to be $(20 \pm 2)\%$. We may determine $R$ using our value for the production of $_{\Lambda}He^4 + \pi^-$ along with two independent measurements, in the same bubble-chamber film, of the branching ratio for $\Lambda + He^3 + \pi^-$: $(9.2 \pm 0.9)\%$ (Ref. 21) and $(11.2 \pm 2.7)\%$ (Ref. 22). We find $R = (9.8 \pm 1.3)\%$ in disagreement with Ref. 10. The discrepancy comes primarily from the production branching ratio for $_{\Lambda}He^4$, since one can infer that Block's number for the production fraction $\Lambda + He^3 + \pi^-$ is $(7.2 \pm 2.2)\%$.

The large experimental discrepancy and the strong model dependence of the theoretical expectation are such as to clearly leave entirely open the question of whether the spin-1 excited state of $_{\Lambda}He^4$ is produced in helium. Thus, the mere observation of hypernuclear production provides no evidence concerning the $\bar{K}\Lambda$ parity. It is shown in the next section, however, that the present determination of $B_{\Lambda}$ at production establishes with high probability that the parity is indeed odd, as expected.

### C. Binding Energies

The measurements of $_{\Lambda}He^4$ binding energies in this experiment are of particular interest for two reasons: It is the first time that they have been measured at production as well as decay, and these are the first measurements not done in emulsion.

The values given in Table V show a binding-

energy difference

$$\Delta B_\Lambda \equiv B_\Lambda^d - B_\Lambda^p = (0.56 \pm 0.46)\ \text{MeV}$$

in the direction to be expected if some ${}_\Lambda\text{He}^4$ were produced in an excited state from which they would deexcite by $\gamma$ emission in a short time compared to the weak decay lifetime. If $f_e$ is the fraction of the ${}_\Lambda\text{He}^4$ events produced in the excited state in the present experiment, we may estimate its value from

$$f_e = \frac{\Delta B_\Lambda}{\Delta E}\ , \tag{10}$$

where $\Delta E$ is the excitation of the excited state. The data yield $f_e = (51 \pm 42)\%$ and $f_e = (40 \pm 32)\%$ using $\Delta E = 1.09$ MeV and $\Delta E = 1.42$ MeV, respectively.

If the excited state of ${}_\Lambda\text{He}^4$ has $J = 1$, the value of $f_e$ is constrained to be zero by angular momentum and parity conservation, for reactions induced by $K^-$ interacting from $s$ states (assuming odd $\bar{K}\Lambda$ parity). Reactions from states of $l \geq 1$, however, allow both spin states of ${}_\Lambda\text{He}^4$ to be produced (again assuming odd $\bar{K}\Lambda$ parity). The data are consistent with roughly equal amounts of $s$- and $p$-state capture.

In view of the difficulties in making background subtractions discussed in Sec. III, it should be noted that the $\pi^- 1P$ topology by itself yields $\Delta B_\Lambda = -0.02 \pm 0.60$ MeV. This topology is kinematically constrained at both production and decay, in contrast to the others listed in Table I, so we expect background to be minimized here. This result is consistent with $\Delta B_\Lambda = 0$ and is 1.9 and 2.4 standard deviations away from 1.09 MeV and 1.42 MeV, respectively. From this it follows that ground-state production is favored and that $\bar{K}\Lambda$ parity is odd, in agreement with the measurements of odd $\bar{K}\Sigma$ (Ref. 23) and even $\Sigma\Lambda$ (Ref. 24) parities.

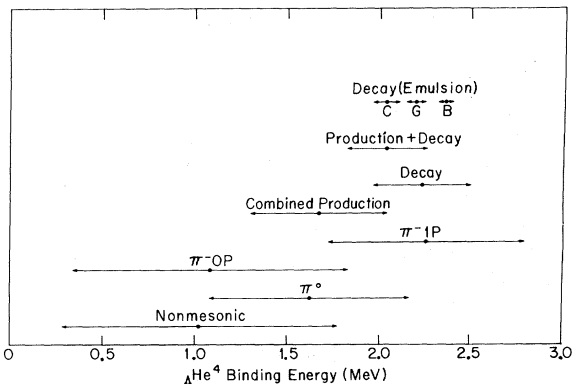


FIG. 12. The binding of ${}_\Lambda\text{He}^4$ as determined in this experiment compared to recent high statistics emulsion values. The binding determined from the production and decay reactions in this work are shown separately, along with their average. The points labeled $C$, $G$, and $B$ are emulsion values from Ref. a in Table VI, Ref. 11, and Ref. 25, respectively.

It is tempting to try to sharpen these conclusions about the $K^-$ capture state and the $\bar{K}\Lambda$ parity by comparing the result of this experiment for $B_\Lambda$ (production) with the more precise results of $B_\Lambda$ (decay) obtained in emulsion. For example, the highest precision result to date is that of Bohm *et al.*[25]: $B_\Lambda(\text{decay}) = 2.36 \pm 0.04$ MeV. Using this value with our $B_\Lambda$(production), we obtain a difference of $0.68 \pm 0.37$ MeV. Compared to the value of 1.09 MeV expected for even $P_{\bar{K}\Lambda}$, this is actually a less decisive result than above. When we calculate $f_e$ by Eq. (10), we find $f_e = 0.62 \pm 0.34$. This (with odd $P_{\bar{K}\Lambda}$) would imply $K^-$ capture in helium predominantly from states of $l \geq 1$.

However, it is risky to use both bubble chamber and emulsion results without allowing additional uncertainty for possible systematic differences between the two techniques. Furthermore, the different emulsion results are known to exhibit systematic deviations among themselves much larger than their quoted statistical errors. For example, the same experiment (Ref. 25) yielded ${}_\Lambda\text{He}^4$ binding energies from two- and three-body decays, respectively, of $2.29 \pm 0.04$ MeV and $2.08 \pm 0.06$ MeV, whose difference of $0.21 \pm 0.07$ MeV is incompatible with zero. A recent study of the range-energy relation in emulsion[26] showed that this difference vanishes if, in the calculation of $B_\Lambda$, one uses for the $\Lambda$ mass a value determined from events where the pion lies in the same range interval as those pions from the decay of ${}_\Lambda\text{He}^4$. These authors[26] conclude that a systematic error of ~0.1 MeV is appropriate for binding energies measured in emulsion.

A summary of the most recent high-precision ${}_\Lambda\text{He}^4$ results is shown in Fig. 12 along with the results of this experiment. There are evidently systematic errors even among the emulsion ${}_\Lambda\text{He}^4$ results which are all determined using the same decay modes. Unfortunately, the decay binding result of the present experiment includes statistical and systematic errors which are too large to distinguish between the different emulsion results.

### D. Ground-State Spin of ${}_\Lambda\text{He}^4$

Although it has long been known that the ground-state spin of ${}_\Lambda\text{He}^4$ is zero,[27] the situation for ${}_\Lambda\text{He}^4$ is less clear. Dalitz and Liu[28] calculated the expected value of

$$R_0 = \frac{\Gamma({}_\Lambda\text{He}^4 \to \pi^0 + \text{any})}{\Gamma({}_\Lambda\text{He}^4 \to \pi^- + \text{any})}$$

for assumed ground-state spins zero and one. This

value also depends on the nonleptonic $\Lambda$ decay parameters, $S_0$ and $P_0$.

Block *et al.*[10] measured $R_0$ to be $2.49 \pm 0.34$, and *assuming* $J=0$, concluded that

$$\frac{P_0^2}{P_0^2+S_0^2} = 0.01^{+0.17}_{-0.01}$$

in agreement with the $\Delta I = \frac{1}{2}$ rule.

Since the ground-state spin of $_{\Lambda}He^4$ has not been measured and since the $\Delta I = \frac{1}{2}$ rule is otherwise reasonably well founded, it seems useful to turn the argument around and use $\Delta I = \frac{1}{2}$ and $R_0$ to determine the spin. The experimental situation is shown in Fig. 13. As indicated, the value of $\alpha_0$ measured in Ref. 29 is consistent with either $P_0^2/(P_0^2+S_0^2) = 0.12 \pm 0.02$ ($\Delta I = \frac{1}{2}$) or $0.88 \pm 0.02$ ($\Delta I \neq \frac{1}{2}$). The present result of $R_0 = 2.20 \pm 0.39$ is combined with the earlier measurement to give $R_0 = 2.36 \pm 0.26$ shown on the figure. If we do not, *a priori*, invoke the $\Delta I = \frac{1}{2}$ rule, it is difficult to distinguish between $P_0^2/(P_0^2+S_0^2) \cong 0.1$ and $J=0$ versus $P_0^2/(P_0^2+S_0^2) \cong 0.9$ and $J=1$. However, if we use $\Delta I = \frac{1}{2}$, then[30]

$$\frac{P_0^2}{P_0^2+S_0^2} = \frac{P^2}{P^2+S^2} = 0.118 \pm 0.007,$$

and the $R_0$ measurements clearly favor $J=0$ for the $_{\Lambda}He^4$ ground state.

Unfortunately, there exists another measurement which tends to the opposite conclusion. Ammar,[31] in nuclear emulsion, measured

$$\frac{\Gamma(_{\Lambda}He^4 \to \pi^0 + He^4)}{\Gamma(_{\Lambda}He^4 \to \pi^- + \text{any})} = 0.7 \pm 0.4.$$

We may combine this with bubble-chamber measurements (see Table VI) of $\Gamma(_{\Lambda}He^4 \to \pi^0 + \text{any})/\Gamma(_{\Lambda}He^4 \to \pi^- + \text{any})$ to determine

$$R_0' = \frac{\Gamma(_{\Lambda}He^4 \to \pi^0 + He^4)}{\Gamma(_{\Lambda}He^4 \to \pi^0 + \text{any})}.$$

The results for $R_0'$ are $0.32 \pm 0.19$ and $0.28 \pm 0.16$ respectively from this experiment and from Ref. 10. These are to be compared to the theoretical results[32] 0.74 and 0.22 respectively for $J=0,1$ which were calculated assuming $\Delta I = \frac{1}{2}$.

Two independent bubble-chamber results for $R_0$ agree, while the emulsion result leading to the determination of $R_0'$ is uncorroborated. The probable conclusion, at this time, seems to be that the ground-state spin is indeed zero.

That this is so has traditionally been inferred from charge symmetry, and the fact that the ground state of $_{\Lambda}H^4$ is spin-zero. However, it appears that there are important charge-symmetry-breaking (CSB) effects (due, e.g., to $\Sigma^0$-$\Lambda$ mixing) which must be taken into account when discussing the hypernuclear energy levels. Downs and Phillips[33] have discussed a potential of the form

$$V_{CSB}(r) = -\tau_3^N(A + B\vec{\sigma}_{\Lambda} \cdot \vec{\sigma}_N) f(r),$$

which will have opposite effects on the binding energies for $J=0$ versus $J=1$ as well as for $_{\Lambda}He^4$ versus $_{\Lambda}H^4$. Attempts to understand the light hypernuclei in detail, including such effects, were discussed by Herndon and Tang.[19] They comment that, although they have assumed the ground-state spin of $_{\Lambda}He^4$ to be zero in their analysis, this really needs to be established experimentally. The theoretical situation is confused due to uncertainties about the nature of the charge-symmetry-breaking forces, three-body forces, and other effects.

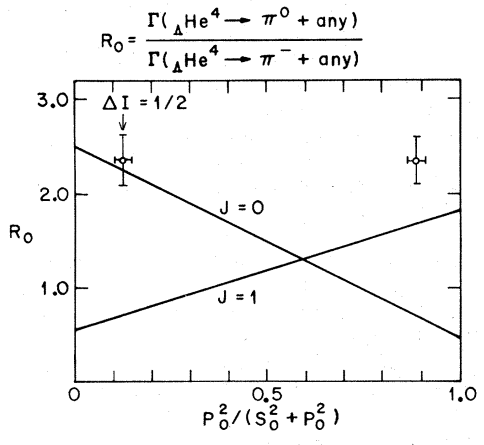


FIG. 13. Decay branching ratio $R_0$ vs $P_0^2/(P_0^2+S_0^2)$. The circles are plotted at values of $R_0$ as determined in the present experiment and Ref. 10. They are plotted at both values of $P_0^2/(P_0^2+S_0^2)$ consistent with the measurement of Ref. 29. The curves show the theoretically expected values of $R_0$ as functions of $P_0^2/(P_0^2+S_0^2)$ for both possible values of ground-state spin. The arrow shows the value of $P_0^2/(P_0^2+S_0^2)$ implied by the results given in Ref. 29 if $\Delta I = \frac{1}{2}$ is assumed in $\Lambda$ decay.

### E. Summary of Conclusions

The decay branching ratios for $_{\Lambda}He^4$ have been measured and are found to be in reasonable agreement with those found in the previous bubble-chamber work. However, we find a discrepancy of nearly a factor of 2 in the production ratio

$$\frac{\Gamma(_{\Lambda}He^4 + \pi^-)}{\Gamma(_{\Lambda}He^4 + \pi^-) + \Gamma(\Lambda + He^3 + \pi^-)}.$$

We have measured the total rate for production of $_{\Lambda}He^4$ by $K^-$ stopped in liquid helium to be $(0.99 \pm 0.09)\%$.

We emphasize that until now, there has been no

evidence on the $\bar{K}\Lambda$ parity from hyperfragment production, due to complete ignorance of whether the excited states are produced when the mass-4 hypernuclei are made in helium. However, we are now able to deduce the $\bar{K}\Lambda$ parity with reasonable certainty by using our measurement of the average value of $B_\Lambda$ at production in conjunction with the recent measurement of the excitation of the excited state of ${}_\Lambda\mathrm{He}^4$. We find the expected result: $P_{\bar{K}\Lambda}$ is odd.

It is worth pointing out that there is still some question regarding the ground-state spin of ${}_\Lambda\mathrm{He}^4$. Although the experimental evidence (assuming $\Delta I = \frac{1}{2}$) seems to favor $J=0$, the situation is somewhat confused by Ammar's emulsion result. This is an important point, since if $J=1$, the foundations of our concepts about $\Lambda N$ forces and the properties of hypernuclei would need to be seriously revised. It would be desirable to have verification of Ammar's measurement of the ${}_\Lambda\mathrm{He}^4$ decay branching $\Gamma(\pi^0+\mathrm{He}^4)/\Gamma(\pi^-+\mathrm{any})$. It would also be interesting to look for $\gamma$ rays from the excited state of ${}_\Lambda\mathrm{He}^4$ produced by stopped $K^-$ in liquid helium. Given odd $\bar{K}\Lambda$ parity and $s$-wave capture, copious excited-state production would indicate that $J=1$ for the ground state. On the other hand, if $J=0$ (ground state), then the (expected small) branching into the excited state would be a measure of the frequency of $K^-$ capture from atomic states of $l \geq 1$, since excited-state production would be forbidden from initial $s$ states.

## ACKNOWLEDGMENTS

The C-MU authors are grateful for the help of D. Zack and C. W. Fette in the initial stages of the experiment. They are especially in debt to J. Rudman for his invaluable efforts in most phases of the analysis. The Argonne film was scanned by Hope Chaffee, Modesta Umbrasas, Chris Dedin, and Joyce Brandalino. We acknowledge the assistance of the ZGS staff in making this experiment possible.

---

*Work supported by the U. S. Atomic Energy Commission.

†On leave at Rutherford High Energy Laboratory, Chilton, Didcot, Berkshire, England.

‡Now at University College, London, England.

§Now at Evansville University, Evansville, Ind. 47714.

||Now at Argonne National Laboratory, Argonne, Ill. 60439.

**Now at Carnegie-Mellon University, Pittsburgh, Pa. 15213.

[1]A general review of properties of hypernuclei is given by D. H. Davis and J. Sacton, in *High Energy Physics*, edited by E. H. S. Burhop (Academic, New York, 1967), Vol. II, p. 365.

[2]The only ambiguity that exists is between ${}_\Lambda\mathrm{H}^3$ and ${}_\Lambda\mathrm{H}^4$ from the production states ${}_\Lambda\mathrm{H}^3 n\pi^0$ and ${}_\Lambda\mathrm{H}^4\pi^0$. A pure sample of ${}_\Lambda\mathrm{H}^3$ can be selected using the production state ${}_\Lambda\mathrm{H}^3 p\pi^-$.

[3]For a complete discussion of this point as well as a general theoretical review of hypernuclear properties, see R. H. Dalitz, in *Nuclear Physics*, edited by C. DeWitt and V. Gillet (Gordon and Breach, London, 1969), p. 703.

[4]G. Keyes, M. Derrick, T. Fields, L. G. Hyman, J. G. Fetkovich, J. McKenzie, B. Riley, and I-T. Wang, Phys. Rev. D 1, 66 (1970).

[5]Scanning and analysis procedures were established independently at Argonne and Carnegie. Where these differed, both are described throughout this paper.

[6]The precision of track measurements in this chamber is discussed in detail in L. G. Hyman, K. O. Bunnell, M. Derrick, T. Fields, P. Katz, G. Keyes, J. G. Fetkovich, J. McKenzie, and I-T. Wang, Phys. Rev. D 5, 1063 (1972).

[7]J. H. E. Mattauch, W. Thiele, and A. H. Wapstra, Nucl. Phys. 67, 1 (1965).

[8]Particle Data Group, Rev. Mod. Phys. 43, S 1 (1971). This result for $M(\Lambda)$ does not include the value from Ref. 6.

[9]M. M. Block, E. B. Brucker, C. C. Chang, R. Gessaroli, T. Kikuchi, A. Kovacs, C. M. Meltzer, A. Pevsner, P. Schlein, R. Strand, H. O. Cohn, E. M. Harth, J. Leitner, L. Monari, L. Lendinara, and G. Puppi, in *Proceedings of the Tenth Annual International Rochester Conference on High-Energy Physics, 1960,* edited by E. C. G. Sudarshan, J. H. Tinlot, and A. C. Melissinos (Interscience, New York, 1960), p. 419

[10]M. M. Block, R. Gessaroli, J. Kopelman, S. Ratti, M. Schneeberger, L. Grimellini, T. Kikuchi, L. Lendinara, L. Monari, W. Becker, and E. Harth, in *Proceedings of the International Conference on Hyperfragments, St. Cergue, 1963* (CERN, Geneva, 1964), p. 63; results on a smaller sample appear in M. M. Block, R. Gessaroli, S. Ratti, L. Grimellini, T. Kikuchi, L. Lendinara, L. Monari, and E. Harth, Nuovo Cimento 28, 299 (1963).

[11]W. Gajewski, J. Sacton, P. Vilain, G. Wilquet, D. Stanley, D. H. Davis, E. R. Fletcher, J. E. Allen, V. A. Bull, A. P. Conway, and P. V. March, Phys. Letters 21, 673 (1966).

[12]H. G. Miller, M. W. Holland, J. P. Roalsvig, and R. G. Sorensen, Phys. Rev. 167, 922 (1968).

[13]M. Rayet, Nuovo Cimento 42B, 238 (1966).

[14]G. Coremans, J. Sacton, D. H. Davis, J. E. Allen, and A. Fishwick, Bulletin de l'Institut de Physique de l'Université Libre de Bruxelles No. 35, 1968 (unpublished).

[15]G. Coremans, J. Sacton, D. O'Sullivan, F. Esmael, D. H. Davis, M. A. Shaukat, T. Pniewski, and J. E. Allen, Nucl. Phys. B16, 209 (1970).

[16]M. M. Block, E. B. Brucker, I. S. Hughes, T. Kikuchi, C. Meltzer, F. Anderson, A. Pevsner, E. M. Harth, J. Leitner, and H. O. Cohn, Phys. Rev. Letters 3, 291

(1959).
[17]R. H. Dalitz and B. W. Downs, Phys. Rev. 111, 967 (1958).
[18]M. M. Block, in *Proceedings of the International Conference on Hyperfragments, St. Cergue, 1963* (CERN, Geneva, 1964), p. 75.
[19]R. C. Herndon and Y. C. Tang, Phys. Rev. 159, 853 (1967). This paper is part of a series including Phys. Rev. 165, 1093 (1968) and Phys. Rev. 153, 1091 (1967). For a recent summary, see Y. C. Tang, in *Proceedings of International Conference on Hypernuclear Physics*, edited by A. R. Bodmer and L. G. Hyman (ANL, Argonne, Ill., 1969), p. 276.
[20]A. Bamberger, M. A. Faessler, U. Lynen, H. Prekarz, J. Piekarz, J. Pniewski, B. Povh, H. G. Ritter, and V. Soergel, Phys. Letters 36B, 412 (1971).
[21]K. Bunnell, M. Derrick, T. Fields, L. G. Hyman, and G. Keyes, Phys. Rev. D 2, 98 (1970).
[22]P. A. Katz, K. Bunnell, M. Derrick, T. Fields, L. G. Hyman, and G. Keyes, Phys. Rev. D 1, 1267 (1970).
[23]Mason B. Watson, Massimiliano Ferro-Luzzi, and Robert D. Tripp, Phys. Rev. 131, 2248 (1963).
[24]H. Courant, H. Filthuth, P. Franzini, R. G. Glasser, A. Minguzzi-Ranzi, A. Segar, W. Willis, R. A. Burnstein, T. B. Day, B. Kehoe, A. J. Herz, M. Sakitt, B. Sechi-Zorn, N. Seeman, and G. A. Snow, Phys. Rev. Letters 10, 409 (1963).
[25]G. Bohm, J. Klabuhn, U. Krecker, F. Wysotski, G. Coremans, W. Gajewski, C. Mayeur, J. Sacton, P. Vilain, G. Wilquet, D. O'Sullivan, D. Stanley, D. H. Davis, E. R. Fletcher, S. P. Lovell, N. C. Roy, J. H. Wickens, A. Filipkowski, K. Garbowska-Pniewska, T. Pniewski, E. Skrzypczak, T. Sobczak, J. E. Allen, V. A. Bull, A. P. Conway, A. Fishwick, and P. V. March, Nucl. Phys. B4, 511 (1968).
[26]G. Bohm, U. Krecker, C. Mayeur, J. Sacton, J. H. Wickens, F. Esmael, D. Stanley, D. H. Davis, J. E. Allen, A. Filipkowski, and E. Skrzypczak, Nuovo Cimento 70A, 384 (1970).
[27]D. Bertrand, G. Coremans, C. Mayeur, J. Sacton, P. Vilain, G. Wilquet, J. H. Wickens, D. O'Sullivan, D. H. Davis, and J. E. Allen, Nucl. Phys. B16, 77 (1970). This paper also contains references to earlier results.
[28]R. H. Dalitz and L. Liu, Phys. Rev. 116, 1312 (1959).
[29]B. Cork, L. Kerth, W. Wentzel, J. Cronin, and R. Cool, Phys. Rev. 120, 1000 (1960); S. Olsen, L. Pondrom, R. Handler, P. Limon, J. A. Smith, and O. E. Overseth, Phys. Rev. Letters 24, 843 (1970).
[30]O. E. Overseth and R. F. Roth, Phys. Rev. Letters 19, 391 (1967).
[31]R. G. Ammar, Nuovo Cimento 14, 1226 (1959).
[32]R. H. Dalitz, private communication.
[33]B. W. Downs and R. J. N. Phillips, Nuovo Cimento 41, 374 (1966).

PHYSICAL REVIEW D VOLUME 6, NUMBER 11 1 DECEMBER 1972

# Production of Charged Pions by 730-MeV Protons from Hydrogen and Selected Nuclei*

D. R. F. Cochran, P. N. Dean, P. A. M. Gram, E. A. Knapp, E. R. Martin, D. E. Nagle, R. B. Perkins, W. J. Shlaer, H. A. Thiessen, and E. D. Theriot†
*University of California Los Alamos Scientific Laboratory, Los Alamos, New Mexico 87544*
(Received 14 February 1972)

An experiment was done in the external proton beam of the Berkeley 184-in. cyclotron to measure the production cross sections for pions from various target nuclei, from hydrogen to lead. The cross-section data are presented and the reaction mechanisms discussed. The hydrogen production appears to fit the one-pion-exchange model.

## I. INTRODUCTION

Pion production cross sections for protons on hydrogen and other nuclei constitute some of the basic data for medium-energy physics, equally important in the theoretical understanding of pion physics and as input for the design of pion beams for the new generation of meson factories now under construction. Many experiments have measured some of these cross sections; however, no experiment had been undertaken which covered a wide range of target materials, production angles, and pion energies.[1-15] In the present work there was enough redundancy in the identification of particles so that counting efficiencies and backgrounds could be accurately measured and taken into account in the computation of cross sections, and so that the proton and electron component in each momentum channel could also be measured. Here we report measurement of the differential cross section for pion production ($d^2\sigma/d\Omega dE$) by 730-MeV protons on H, D, Be, C, Al, Ti, Cu, Ag, Ta, Pb, and Th at eleven lab angles in the interval 15°–150° and at twelve energies in the interval 25–550 MeV. The vast amount of data represented by this matrix of parameters required automatic data handling and reduction, which was accomplished using an on-line digital computer, with data reduction simultaneously done during the experiment. The experiment used the external proton beam of the